Positron trapping at precipitates in Au-26.5 at.% Pt

1995 J. Phys.: Condens. Matter 7 5939

(http://iopscience.iop.org/0953-8984/7/29/020)

J. Phys.: Condens. Matter 7 (1995) 5939–5947. Printed in the UK

Positron trapping at precipitates in Au–26.5 at.% Pt

W Pahl†, V Gröger†, G Krexner‡ and A Dupasquier§

† Institut für Festkörperphysik der Universität Wien, Strudlhofgasse 4, A-1090 Wien, Austria
‡ Institut für Experimentalphysik der Universität Wien, Strudlhofgasse 4, A-1090 Wien, Austria
§ Dipartimento di Fisica, Politecnico di Milano, Piazza Leonardo da Vinci 32, I-20133 Milano, Italy

Received 28 December 1994, in final form 9 May 1995

Abstract. The precipitation kinetics of the Au–26.5 at.% Pt alloy, quenched within the miscibility gap and annealed isothermally at 900 K, was studied by positron annihilation spectroscopy (PAS) using the lifetime technique as well as the Doppler broadening technique. Information on the size of the platinum-rich precipitates was obtained from small-angle neutron scattering (SANS) measurements. The results of the PAS measurements were interpreted by assuming that a fraction of the positrons, depending on the morphology of the material, is trapped at misfit dislocations on the boundaries of platinum-rich precipitates. The positron trapping rate per unit specific area of the interphase boundary was obtained by combining PAS data with SANS results. The discussion points out the importance of this parameter and of the positron lifetime data for a characterization of the local structure of the interphase boundary. By assuming that the growth kinetics of the platinum-rich precipitates is governed by a $t^{1/3}$ law, we obtain from our data quantitative information on the shape of the size distribution of the precipitates.

1. Introduction

Positron annihilation spectroscopy (PAS) is increasingly used for investigations of phase boundaries [1] and precipitation kinetics [2, 3]. Most promising for simplicity are systems

—with a large miscibility gap, causing nearly pure metal to be precipitated
—containing only one kind of positron trapping centre.

The AuPt alloy (26.5 at.% Pt), studied in the present work, fulfils the above conditions. The decomposition of the supersaturated AuPt system during thermal ageing at 900 K produces a distribution of nearly spherical precipitates with a Pt atomic concentration of 98% [4], dispersed in a matrix of Au–19.5 at.% Pt. Due to the difference in the lattice parameter of the Pt-rich precipitates and of the matrix (about 4%), a transition from coherent to semicoherent particles is expected in the precipitation sequence. The misfit regions at the boundaries between semicoherent particles and matrix are most likely to act as extended positron trapping centres. Indeed, these are the only positron traps expected to exist in AuPt samples after the first stages of thermal ageing, i.e. when the vacancies and vacancy clusters, frozen into the sample with the homogenization treatment, are already annealed out. Positron trapping in the volume of the Pt-rich precipitates can be excluded due to a significantly larger positron affinity to the Au-rich matrix [5].

As discussed below, in these ideal conditions the analysis of PAS data can be fertile with information regarding (a) the shape of the size distribution of the precipitates, (b) the law of evolution of this size distribution, (c) the critical time marking the transition from coherent to semicoherent precipitation and (d) the structure of the particle–matrix interface. Moreover, with the help of a determination of the average particle size, which in the present case was obtained by an auxiliary small-angle neutron scattering (SANS) measurement, it is also possible to give an estimate of the positron trapping rate per unit specific area of the interphase boundary. This parameter can be taken as a characteristic property related to the structure of the boundary.

2. Experimental details

Pure gold and platinum (26.5 at.%) of purity 4N were melted in an induction furnace in argon atmosphere. The alloy was directly quenched from the liquid state into a water-cooled ingot with a parabolic end piece. After rolling to about one-half of the thickness, the samples were homogenized at 1373 K for 7 days with subsequent water quench. For the positron measurements the samples were rolled to the final thickness of about 0.2 mm and cut in 6×6 mm^2 squares, and again homogenized. Composition and homogeneity were checked by microprobe and by measurements of the electrical resistivity by a four-point method. The samples were then isothermally annealed at 900 K for different times.

For PAS measurements, two identical samples were sandwiched with a 3×10^5 Bq ^{22}Na positron source, evaporated onto a 1.14 mg cm^{-2} Kapton foil. The lifetime measurements were carried out using a fast–slow coincidence system with a resolution of 220 ps in operating conditions. The γ detectors were mounted at an angle of 135° to avoid the systematic underestimate of the lifetimes that might be given by false prompt coincidences, which are likely to occur when the detectors are aligned. The spectra, containing at least 5×10^6 counts each, were analysed by the RESOLUTION and POSITRONFIT computer programs [6, 7]. After source and background corrections we could fit well all spectra with one or two components, depending on the ageing time. For well annealed specimens of pure gold and pure platinum we obtain one-component spectra with lifetimes of 127 ± 1 ps and 115 ± 1 ps respectively. The Doppler-broadened energy spectrum of the annihilation radiation was measured using a high-purity Ge detector with energy resolution of 1.2 keV and a channel width of 25.9 eV. Eighty central channels out of 600 were used for the determination of the S parameter [8]. We report below the results of our Doppler broadening measurements in terms of normalized parameters S/S_{Au}, where $S_{Au} = 0.5371$ is the value found for well annealed pure gold; for well annealed pure platinum we obtain $S_{Pt}/S_{Au} = 0.9825$.

As discussed below, additional information on the average radius of the precipitates is necessary for the complete interpretation of the PAS data. As the contrast conditions are not favourable for x-ray scattering, SANS measurements at neutron wavelengths of 0.4 nm and 0.8 nm were performed at the spectrometre PAXE in Saclay.

3. Results and discussion

The S parameter for the series of samples aged at 900 K, divided by the S parameter for pure gold, is plotted in figure 1 versus the ageing time, t. The statistical error (of the order of 3×10^{-4} for S and 5×10^{-4} for S/S_{Au}) is smaller than the data points of the figure. However, the data obtained for different samples may scatter due to unavoidable differences in the sample preparation. This will also apply to the lifetime data discussed below. The arrows in figure 1 mark the levels of three reference points: pure gold, pure platinum, and homogenized alloy. The latter level includes a contribution characteristic of positron trapping at vacancies, which are the dominating defect species in the sample after the rapid quenching from the homogenization temperature. The full line through the data points is the result of the model calculation discussed below. Note that, after ageing for times below 200 min, the S parameter remains nearly constant at a value close to the mean value between pure gold and pure platinum, weighted on the atomic fractions at the equilibrium concentration of the matrix at the ageing temperature. This result, expected for positrons uniformly delocalized over a large number of atomic cells of a random dilute solution, is consistent with the hypothesis that at this stage there is no positron trapping at lattice defects. However, for longer annealing times ($t > 200$ min), trapping is made clear by the increase of the S parameter. At about 2000 min, the S curve reaches a maximum, which is well below the value found for the homogenized (quenched) sample. Taken by itself, this result could be explained in different ways: either that the traps in the annealed samples are defects with a free volume smaller than a vacancy, or that the maximum fraction of positrons trapped in annealed samples is smaller than the fraction trapped in a quenched sample, or else a combination of both circumstances. We shall see below that the third possibility is the only one compatible with the lifetime results. For

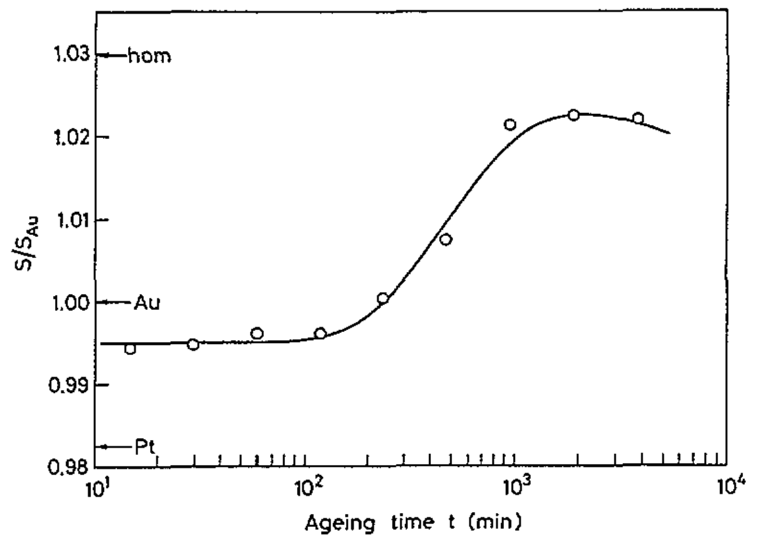

Figure 1. Normalized S parameter in AuPt aged at 900 K, as a function of the ageing time. The values for pure gold, pure platinum, and homogenized alloy are indicated by arrows; the S parameter for pure gold, taken as the reference level for the normalization, is $S_{Au} = 0.5371$. The statistical error is approximately of the order of the symbol size. The curve is the result of the best-fit calculation described in the text.

samples aged less than 200 min, the lifetime spectra could be fitted by one component only. The lifetime $\tau_b = 125 \pm 1$ ps is close to the weighted mean between gold and platinum lifetimes. In accordance with S measurements, this result demonstrates the absence of positron trapping defects in the initial stages of ageing. In contrast, for annealing times above 200 min, the effect of positron trapping becomes manifest: in this case, the fitting of the lifetime spectra requires a second component, that will be referred below as the 'defect component'. The lifetime τ_d of this component is approximately the same for all samples ($\tau_d = 175 \pm 3$ ps), and is definitely shorter than the long lifetime measured with the quenched sample ($\tau_v = 195 \pm 5$ ps). The intensity I_d of the defect component reaches

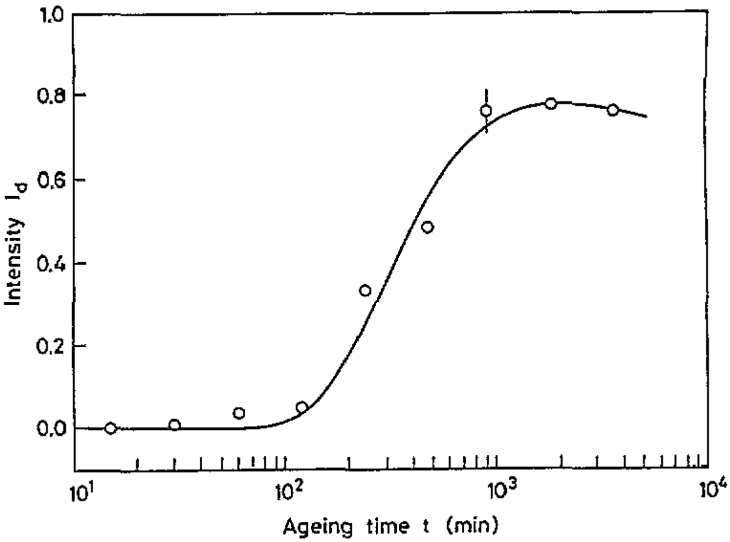

Figure 2. Intensity I_d of the long-living component of the positron lifetime spectrum in AuPt aged at 900 K, as a function of the ageing time. The curve is calculated using the best-fit parameters obtained on the basis of the data in figures 1 and 3.

a maximum of $77 \pm 5\%$ after ageing above 1000 min (see figure 2). This behaviour is again consistent with the Doppler broadening results, but in this case there is no possible ambiguity regarding the interpretation. The result $\tau_d < \tau_v$ shows that the positron traps present in the aged samples are defects with less local free volume than a vacancy; also, the maximum of I_d below 100% indicates that the trapping process never reaches a saturation stage (a maximum intensity of 77% corresponds to a trapping probability of only about 49%). Figure 3 shows the dependence on the ageing time of the mean lifetime $\bar{\tau}$, as calculated from the results of the two-component spectrum analysis. As is well known, the virtue of this parameter is to be more accurate than the direct results of the analysis (a few typical error bars shown in figure 3 represent the overall statistical fluctuation, without including the effect of accidental differences in the thermal treatments). Note that the curves of figures 1 and 3 are identical: this is obtained by a simple rescaling of the vertical axes, and shows that the independent measurements of S and $\bar{\tau}$, which give the same physical information, are in perfect agreement. The points in figures 1 and 3 were used for the best-fit adjustment of the model curves. We interpret our results by assuming that the positrons are captured at the interphase boundaries between Pt-rich precipitates and matrix. The constant value of the defect lifetime τ_d indicates that the local morphology of the traps probed by positrons does not change during ageing, in spite of the fact that the dimensions of the particles certainly increase. This is not in contrast with our interpretation, since the wavefunction of a trapped positron is enhanced at the spikes of free-volume concentration, and the growth of the particle–matrix interface may occur with an increase of the number of the spikes but with no substantial change of their structure. Considering that the lifetime difference $\tau_d - \tau_b = 50 \pm 3$ ps measured in the present case is close to the value (48 ps) attributed by Shirai *et al* [9] to positrons trapped at Shockley dislocations in pure gold, our results suggest identifying the free-volume spikes with cores of Shockley dislocations (partial dislocations). We may thus represent the interphase boundary as a more or less regular grid of partial dislocation lines. The mesh of the grid must be adequate to relax the elastic deformation due

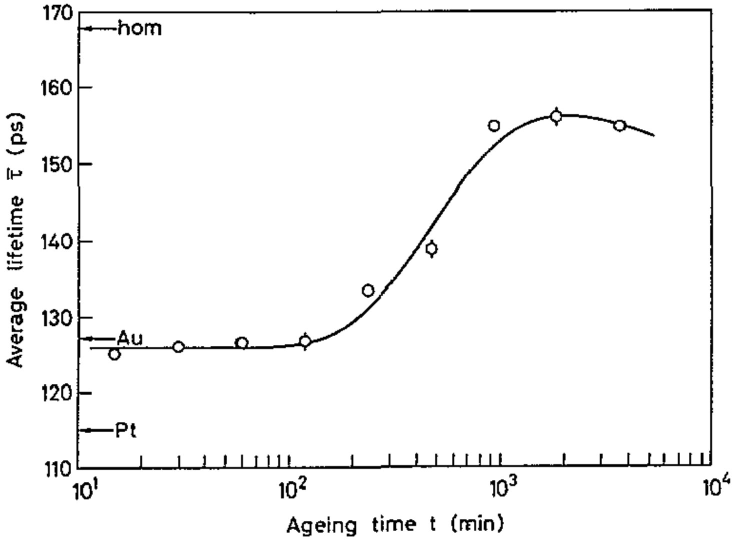

Figure 3. Positron mean lifetime in AuPt aged at 900 K, as a function of the ageing time; the values for pure gold, pure platinum and homogenized alloy are indicated by arrows. The curve is the result of the best-fit calculation described in the text.

to the 4% misfit between the precipitates and the matrix. Using for the Burgers vector of the dislocations the value for Shockley dislocations in gold ($b \approx 0.16$ nm), we calculate a mesh of the order of $L = b/0.04 \approx 4$ nm. Since L is smaller than the wavelength of a thermal positron at room temperature ($\lambda_{th} = 6.2$ nm), the dislocation grid must be considered in the positron trapping process as a bidimensional continuum. Therefore, the correct way of expressing in quantitative form the trapping power of the interphase boundary is to define the trapping rate per unit specific surface ν_s, a parameter with the dimensions of a velocity. The product of ν_s times the specific surface σ (area of trapping surface per unit volume) gives the trapping rate, i.e. one of the key factors determining the fraction of positrons trapped at interphase boundaries (the other factor is the probability that a free positron injected at random in the sample hits the capturing surface during its thermal random walk; we shall see below, however, that, in the present case, this factor is less important than ν_s). In spherical geometry, σ depends on the radius r of the particles and on the volume fraction f occupied by these particles, according to the relationship $\sigma = 3f/r$ (however, $\sigma = 0$ for r smaller than a critical dimension r_c of the order of $L/2 = 2$ nm, representing the maximum radius of coherent particles). Assuming that ν_s is not affected by changes of r occurring during the ageing, we may easily read the evolution of σ into the PAS results as follows:

(a) incubation stage ($t < 200$ min): no trapping, since the radius of the Pt particles is still smaller than r_c and σ is zero,

(b) rapid increase of the trapped fraction (200 min$< t <$ 1000 min): an increasing number of Pt particles reaches the critical radius r_c; σ jumps from zero to its maximum value, of the order of $\sigma_{crit} = 3f/r_c \approx 10^8$ m^2 m^{-3} ($f = 8.9\%$ in equilibrium at the temperature of ageing),

(c) region of the maximum and beginning of a slow decrease of the trapped fraction ($t > 1000$ min): the average radius $\langle r \rangle$ of the particles is now well above r_c, and continues to grow; σ decreases in inverse proportion to $\langle r \rangle$.

The above qualitative description can be converted to mathematical terms with the help of some simplifications. In the appendix we present our approach in detail, but here we prefer to jump to the final results of the analysis and to discuss their information content under two aspects; (a) kinetics of the alloy decomposition and (b) structure of the interphase boundary.

As far as regards the kinetics of decomposition of the alloy, we can tell that our experimental results are in agreement with the following assumptions of the model.

(a) After the initial part of the incubation stage, the volume fraction of the precipitates does not change during ageing.

(b) The average radius $\langle r \rangle$ of the precipitates increases with the ageing time t according to a $t^{1/3}$ law, as predictable for a coalescence regime and in accordance with the experimental results of [4].

(c) The radius distribution of the particles can be scaled to an universal curve by dividing the r axis by $\langle r \rangle$. We have given a convenient analytical form for this distribution and kept the relative width δ as an adjustable parameter. Our best-fit value for δ is $36 \pm 6\%$.

(d) The loss of coherency of the Pt-rich particles occurs when the particles attain a critical radius r_c; in our fitting procedure, we have used as an adjustable parameter the critical time t_c defined by the equation $\langle r(t_c) \rangle = r_c$, and obtained the best-fit value $t_c = 600 \pm 50$ min. The corresponding value of the critical radius is $r_c = 1.3 \pm 0.1$ nm, in fair agreement with the approximate evaluation $r_c \approx L/2 = 2$ nm.

Information on the structure of the interphase boundaries comes from the best-fit determination of the trapping rate per unit specific surface ν_s, for which we obtain the value 70 ± 7 m s^{-1}. This is a quite small value, if compared to the value found for the surface of grain boundaries in various fine-grained alloys (from 200 to 3000 m s^{-1} [10]). The large difference, however, seems reasonable if one compares the high level of incoherence that can be found at the interface between microcrystals of random orientation with the rather regular structure of an interface developed for a gradual loss of coherency between regions with the same orientation and a lattice misfit of only 4%. We see from this comparison that ν_s is a convenient parameter for characterizing the disorder at an internal surface. In the present case, the low value of ν_s essentially tells us that the average free volume localized at the interphase boundary is small. Note, however, that the information on the average free volume is different from, and complementary to, the information on the local free volume at the annihilation site which is given by the measurement of τ_d. As already discussed, the local free volume is not evenly distributed over the surface of the precipitates, but is concentrated on sites structurally equivalent to partial dislocations, spaced at intervals of the order of 4 nm.

Acknowledgements

Support by the grant of the FWF No S 5603 is gratefully acknowledged. We would like to thank H Seidl for help with the sample preparation in connection with FWF grant No S 5605. We are indebted to P Folegati for stimulating discussions. For the SANS measurements, we thank M Prem.

Appendix. Mathematical treatment

If we want to describe positron trapping in analytical terms, the complicated geometry of a real sample containing a distribution of precipitates must be drastically simplified. To this end, we imagine the sample as divided into independent spherical domains of radius R, chosen with the following conditions: (a) a spherule of the Pt-rich phase, having a radius r, is contained at the centre of each domain, (b) the ratio of the volume of the internal spherule to the volume of the domain is equal to the volume ratio f of the Pt-rich phase in the whole sample; this condition implies the relationship $R = r/f^{1/3} = 2.24r$. If one neglects the net current of thermal positrons between adjacent domains, the intensity of the long-living component in the lifetime spectrum (I_d) can be calculated as a function of r, of ν_s, and of the positron diffusion constant D_+ using the diffusion trapping model (DTM) in the version elaborated by Nieminen *et al* [11]. This version, originally formulated for studying positron trapping in voids, can be adapted without formal modification to the present situation, where the void is substituted by a particle with a positron affinity too low to sustain a population of thermal positrons. The application of the DTM normally requires the numerical evaluation of the sum of a series; examples of DTM results are given in figure 4, where the intensity I_d of the long-living component is plotted versus r for a choice of D_+ and ν_s values, and for $R = r/f^{1/3}$. The figure shows that, in the range of D_+ values characteristic of metals and other non-polar solids ($D_+ \approx 10^{-4}$ m^2 s^{-1}) and for $\nu_s < 1000$ m s^{-1}, the intensity I_d in the region $r < 100$ nm is almost insensitive to D_+ (transition-limited regime). Considering that the lifetime results indicate that ν_s cannot be too different from $\lambda_{bulk}/\sigma_{\max} \approx 50$ m s^{-1}, and that the SANS results show that the average radius of the particles is of the order of a few nanometres (we have from SANS an average radius of 1.2 ± 0.1 nm after ageing for 500 min), we can safely assume that the conditions of the transition-limited regime are fulfilled in the case that we are discussing. In these conditions, the DTM results coincide with the well known equations derived from the standard trapping model (STM):

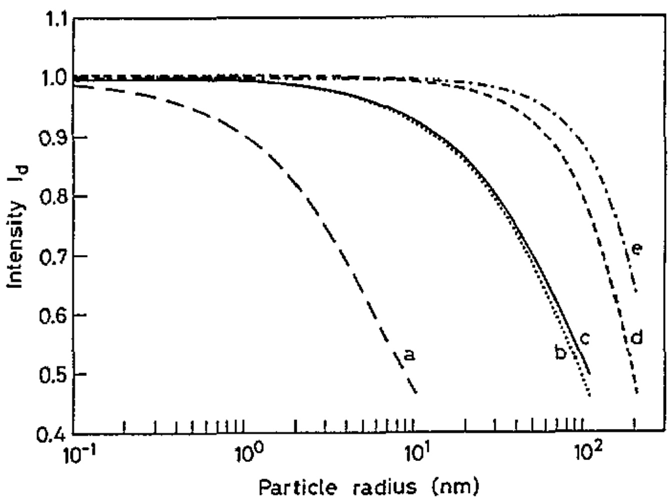

Figure A1. Intensity I_d according to the diffusion trapping model as a function of the particle radius for: (a) $\nu_s = 70$ m s^{-1}, $D_+ = 1 \times 10^{-4}$ m^2 s^{-1} and $D_+ = 2 \times 10^{-4}$ m^2 s^{-1}; (b) $\nu_s = 1000$ m s^{-1}, $D_+ = 1 \times 10^{-4}$ m^2 s^{-1}; (c) $\nu_s = 1000$ m s^{-1}, $D_+ = 2 \times 10^{-4}$ m^2 s^{-1}; (d) $\nu_s = \infty$, $D_+ = 1 \times 10^{-4}$ m^2 s; (e) $\nu_s = \infty$, $D_+ = 2 \times 10^{-4}$ m^2 s. For all curves, $R/r = 2.24$.

$$I_d = \frac{k}{\lambda_{bulk} + k - \lambda_d} \tag{A1}$$

where

$$k = \nu_s \sigma = 3\nu_s f/r \tag{A2}$$

when $r > r_c$ (when $r < r_c$ there is no trapping).

Equations (A1) and (A2) give I_d as a function of r; however, the radius of the particles is a statistical variable depending on the ageing time, and the value of $I_d(t)$ for a sample at a given stage of ageing must be obtained by averaging over the size distribution. Taking into account that the probability that a positron is implanted in a specific domain is proportional to the volume of the domain, we obtain

$$I_d(t) = \int_{r_c}^{\infty} I_d(r) r^3 p(r,t)\,\mathrm{d}r \bigg/ \int_0^{\infty} r^3 p(r,t)\,\mathrm{d}r \tag{A3}$$

where $p(r, t)$ is the size distribution of the Pt particles after ageing for a time t.

STM relationships were used for calculating S and $\bar{\tau}$ from I_d and fitted to the data reported in figures 1 and 3. We adopted a best-fit procedure based on a parametrization of $p(r, t)$ as given by the equation

$$p(r,t) = -\frac{\mathrm{d}}{\mathrm{d}r} \exp\left[-\left(\frac{r}{r_0}\right)^n\right]. \tag{A4}$$

In equation (A4), the time dependence of $p(r, t)$ is implicitly accounted for by assuming that the characteristic radius r_0 increases with the ageing time. The constant n and the radius r_0 are related to the mean radius $\langle r\rangle$ and to the relative width δ of the distribution $p(r, t)$ as follows:

$$\langle r\rangle = r_0 \frac{\Gamma(1/n)}{n} \tag{A5}$$

$$\delta = \frac{\sqrt{\langle(r-\langle r\rangle)^2\rangle}}{\langle r\rangle} = \sqrt{\frac{2n\Gamma(2/n)}{[\Gamma(1/n)]^2} - 1}. \tag{A6}$$

Equation (A6) shows that δ does not depend on the ageing time, but only on the constant n. We treated n as an adjustable parameter (together with ν_s and t_c), and we fixed the dependence of r_0 on the ageing time according to the proportionality law

$$r_0 = a\,t^{1/3}. \tag{A7}$$

The information $\langle r\rangle = 1.2 \pm 0.1$ nm for $t = 500$ min (from SANS) was taken into account for fixing a in accordance with equations (A5) and (A7). This gives the constraint

$$a\frac{\Gamma(1/n)}{n} = 0.15 \text{ nm min}^{-1/3}. \tag{A8}$$

The use of this additional information on the size of the Pt particles is essential for isolating ν_s from σ in the analysis of PAS data. In contrast, n is scarcely affected by any information concerning particle sizes, and is essentially related to the slope of the I_d curve in the stage of rapid increase; the best-fit value with our data is $n = 3 \pm 0.5$, corresponding to $\delta = 36 \pm 6\%$. This result is not independent of the assumption expressed by (A7) (a slower increase of the mean radius with the ageing time would be compensated by a sharper radius distribution, i.e. a smaller δ). The agreement of our experimental result with the value of δ calculated from the Lifshitz–Slyozov–Wagner distribution [12, 13] thus provides *a posteriori* an indirect check of (A7). The other best-fit values are $\nu_s = 70 \pm 7$ m s^{-1} and $t_c = 600 \pm 50$ min. The corresponding critical radius is $r_c = 1.3 \pm 0.1$ nm; here the error reflects the indetermination of the SANS measurement used for fixing the constant a in equation (A7).

References

[1] Gröger V, Fratzl P, Pahl W, Paris O, Bischof G and Krexner G 1995 *Acta Metall. Mater.* **43** 1305
[2] Abis S, Biasini M, Dupasquier A, Sferlazzo P and Somoza A 1989 *J. Phys.: Condens. Matter* **1** 3679
[3] Abis S, Bartolomei P, Biasini M, Dupasquier A and Valli M 1992 *Phys. Status Solidi* a **129** 143
[4] Glas R, Blaschko O and Rosta L 1992 *Phys. Rev.* B **46** 5972
[5] Puska M J, Lanki P and Nieminen R M 1989 *J. Phys.: Condens. Matter* **1** 6081
[6] Kirkegaard P and Eldrup M 1974 *Comput. Phys. Commun.* **7** 401
[7] Kirkegaard P, Eldrup M, Mogensen O E and Pedersen N J 1981 *Comput. Phys. Commun.* **23** 307
[8] Campbell J L 1977 *Appl. Phys.* **13** 365
[9] Shirai Y, Matsumoto K, Kawaguchi G and Yamaguchi M 1992 *Mater. Sci. Forum* **105–110** 1225
[10] Dupasquier A, Romero R and Somoza A 1993 *Phys. Rev.* B **46** 5972
[11] Nieminen R M, Laakkonen J, Hautojärvi P and Vehanen A 1979 *Phys. Rev.* B **19** 1397
[12] Lifschitz M and Slyozov V V 1961 *J. Phys. Chem. Solids* **19** 35
[13] Wagner C 1961 *Z. Elettrochem.* **65** 581